Korean J. Chem. Eng., 35(10), 2138-2144 (2018)
DOI: 10.1007/s11814-018-0111-z

pISSN: 0256-1115
eISSN: 1975-7220

Scalable synthesis of carbon-embedded ordered macroporous titania spheres with structural colors

Dae-Woong Jung*, Kyung Jin Park, Seungwoo Lee*,**, Jaeyun Kim*, Gaehang Lee***, and Gi-Ra Yi*,†**

*Department of Chemical Engineering, Sungkyunkwan University, Suwon 16419, Korea
**SKKU Advanced Institute of Nanotechnology (SAINT), Sungkyunkwan University, Suwon 16419, Korea
***Korea Basic Science Institute, Daejeon 34133, Korea
(*Received 3 May 2018 • accepted 24 June 2018*)

Abstract−Carbon-embedded ordered macroporous titania (C-MAC TiO_2) spheres are prepared in solution by the cooperative self-assembly of polymer beads and a titania precursor within evaporative emulsions and subsequent direct carbonization. Because the highly reactive titania precursors are easily crosslinked to form gels early in evaporation before the polymer beads are self-organized, non-reactive toluene-in-formamide emulsions are used. These non-aqueous emulsions should be stable at relatively high temperatures (~80 °C) for the evaporation process. We found that amphiphilic triblock copolymers of poly(ethylene oxide) (PEO) and poly(phenylene oxide) (PPO) with longer PEO chains (Pluronic® F108 (EO_{125}-b-PO_{64}-b-EO_{125}) are required to stabilize those non-aqueous emulsions, and become more important at higher concentrations used for bulk fabrication. The carbon inside our C-MAC TiO_2 significantly suppresses strong multiple scattering from structural defects or imperfections, thus emphasizing their Bragg reflection colors.

Keywords: Inverse Opal, Titania, Macropore, Structural Color, Sphere

INTRODUCTION

Colloidal particles can be assembled into crystalline structures that may show structural colors corresponding to their optical stop bands, as shown in opal gemstones and *Cotinga maynana* feathers [1,2]. Moreover, hollow colloidal particles can show structural color upon self-assembly [3]. The manipulation of light in such colloidal photonic structures is important in integrated optoelectronic devices [4]. In addition, their highly reflective colors are significant in the development of colorimetric sensors and electronic papers [5,6]. For better mechanical stability, inverse opal structures and ordered macroporous structures are also fabricated by templating colloidal crystals of polymer beads with metal oxides such as silica, titania, tin dioxide, and alumina [7-10]. In particular, the highest-refractive-index non-absorbing material of titania has been extensively explored for inverse opal structures because it may show strong Bragg reflections with fewer layers. Because of the high specific surface areas and semiconducting properties of colloidal crystals of metal oxides, they have been implemented for various applications such as catalytic supporters, photocatalysts, sensors, water-splitting, and dye-sensitized solar cells [11-15]. However, because of imperfections or defects within macroporous titania, multiple scattering dominates Bragg-reflected colors; it is even stronger for materials with high index mismatches (e.g., TiO_2-Air) [16], which appear white in most cases.

In this article, we report the synthesis of carbon-embedded macroporous titania (C-MAC TiO_2) spheres in solution by the evaporation-induced cooperative assembly of polystyrene (PS) beads and titania precursor inside toluene-in-formamide emulsions with subsequent direct carbonization. Because of the broadband light absorption of carbon [17], multiple scattering from structural defects, which is independent of wavelength, can be significantly suppressed. Recently, carbon black nanoparticles were included to suppress multiple scattering in colloidal glasses and crystals [18-20]. In our approach, hydrocarbons within the materials were directly converted into carbon without disturbing the colloidal structures. To prepare macroporous titania spheres, toluene-in-formamide emulsions with PS and titania precursors were used in previous reports [21,22] in which amphiphilic triblock copolymers (Pluronic® P123) were used as stabilizers for the non-aqueous emulsions at relatively lower concentrations. However, we found that the P123 surfactant with short poly (ethylene oxide) (PEO) chains was insufficient to stabilize emulsions at high concentrations or large scales at relatively high temperatures for the evaporation process. Pluronic® F108, having longer PEO chains, could stabilize concentrated non-aqueous emulsions even at high evaporation temperatures.

EXPERIMENTAL

1. Materials

Sodium hydrogen carbonate ($NaHCO_3$, 99%) and formamide (98.5%) were purchased from Junsei. PEO-*b*-PPO-*b*-PEO (EO_{125}-$PO_{64}EO_{125}$, Pluronic® F108, M_w=14,600 g/mol), 4-styrenesulfonic acid sodium salt hydrate (NaSS), divinylbenzene (DVB, 55%), and titanium butoxide (TBT, 97%) were purchased from Aldrich. Potassium persulfate (KPS), toluene (99.5%), and styrene monomers

†To whom correspondence should be addressed.
E-mail: yigira@skku.edu

(99.5%) were purchased from Samchun. All reagents and solvents were used as received without any purification.

2. Synthesis of Crosslinked PS Beads

Crosslinked PS beads were synthesized by emulsifier-free emulsion polymerization. Typically, $NaHCO_3$ (0.75 g), DVB (0.5 g), NaSS (0.1 g), and styrene (35 g) were dissolved in 430 mL of deionized water. Then, the mixture was heated and stirred at 70 °C while purging with nitrogen gas. In 30 min, 0.1 g KPS was carefully introduced as an initiator into the mixed solution, which was stirred for 24 hours at 70 °C under nitrogen atmosphere.

3. Preparation of C-MAC TiO_2 Spheres

The suspension of cross-linked PS beads in toluene (1 wt%, 1 mL) was mixed with 0.01 g TBT and stirred for 30 min, before emulsifying with formamide (0.98 g) and amphiphilic triblock copolymers (Pluronic® F108, 0.2 g) using a mechanical homogenizer (IKA) at 5,000 rpm for 30 s. While annealing the sample at 80 °C for 24 h, the toluene was removed and the hydrolyzed TBT was condensed, yielding composite spheres of PS beads and TiO_2. The composite spheres were washed with ethanol and water four times by gentle centrifugation and re-dispersion. C-MAC TiO_2 spheres were produced by heat treatment under nitrogen atmosphere for 6 h at 540, 700, 800, or 900 °C.

4. Characterization

The shapes and pore structures of the C-MAC TiO_2 spheres were observed by field-emission scanning electron microscopy (FE-SEM; JEOL, JSM-7500F, Japan) and high-resolution transmission electron microscopy (HR-TEM; Tecnai, G2F30). The reflection spectra of the C-MAC TiO_2 spheres were measured using a fiber-coupled spectrophotometer (Ocean Optics Inc., BH-2000-BAL). For in-depth analysis of the reflection spectrum from a single C-MAC TiO_2 sphere, custom-built spectroscopic microscopy was performed, equipped with an imaging spectrometer (IsoPlane, Princeton Instruments) and a charge-coupled device (CCD) camera (PIXIS-400B, Princeton Instruments) on an optical microscope (Nikon Eclipse). The cross-sections of the PS-TiO_2 spheres were prepared and observed by focused ion beam (TESCAN, LTRA3 XMC). The crystal phases were measured by high-resolution X-ray diffractometry (XRD; Discover, D8). The carbon content was measured using an elemental analyzer (Elementar Analysensysteme GmbH, Elementar Vario EL cube).

RESULTS AND DISCUSSION

1. Scalable Synthesis of C-MAC TiO_2 Spheres

As shown in Fig. 1, the suspension of crosslinked PS beads and TiO_2 precursor (TBT) in toluene is emulsified into formamide instead of water because of the high reactivity of TBT in water. Then, emulsions are annealed at the relatively high temperature of ~80 °C for the slow evaporation of toluene through the formamide into the air. This induces the co-assembly of PS beads within the emulsions, producing composite balls of PS beads and amorphous TiO_2. Finally, the composite balls of PS and TiO_2 are heat-treated at ≥540 °C under nitrogen atmosphere. During the heat treatment process, the hydrocarbons within the amorphous titania or PS are decomposed; some of them are directly converted into carbon inside the polycrystalline anatase titania matrix, which yields C-MAC TiO_2 spheres.

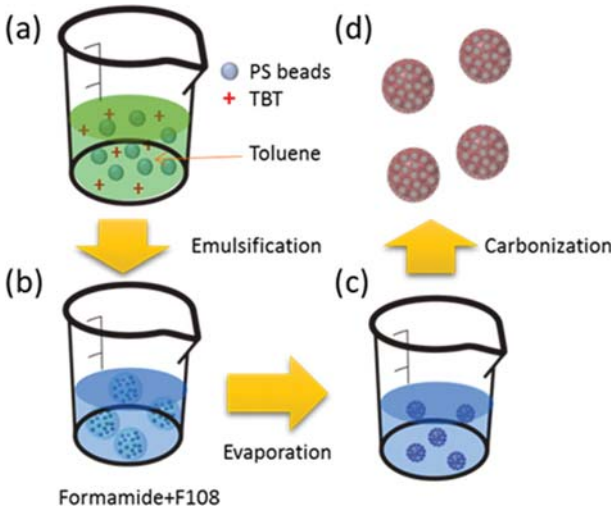

Fig. 1. Scheme of synthesis of C-MAC TiO_2 spheres. (a) TBT and PS beads are dispersed in toluene and (b) the toluene dispersion is emulsified into formamide by a homogenizer. (c) The emulsions are heated and annealed at 80 °C in order to remove toluene, yielding composite spheres of PS-TBT. (d) Finally, C-MAC TiO_2 spheres are obtained by carbonization under nitrogen atmosphere.

In Fig. S1, the PS-TiO_2 composite balls and TiO_2 spheres without carbon both show bright white colors because of multiple scattering, which is much stronger than the structural color induced by Bragg reflection. However, in our carbon-embedded spheres, the structural color appears clearly in the visible region because multiply scattered light is significantly suppressed via effective absorption in the embedded carbon.

Because non-aqueous emulsions are unusual, it is challenging to choose proper surfactants to stabilize them. At low concentrations, several surfactants were reported for stabilization at room temperature in a previous article [21]. We first tried triblock copolymers with short PEO brushes (Pluronic® P123, EO_{20}-PO_{70}-EO_{20}) as a stabilizer for a high-concentration emulsion. However, at high concentrations, stabilization was not achieved. Instead, the emulsion became even more unstable during evaporation at ~80 °C. By contrast, another surfactant with longer PEO brushes (Pluronic® F108) could stabilize the toluene-in-formamide emulsions at relatively high concentrations (>20 vol%) and high temperatures (>80 °C), as shown in Fig. 2.

Through the slow evaporation of the highly stable toluene-in-formamide emulsion with F108, composite spheres of TBT and PS beads were formed; C-MAC TiO_2 spheres were prepared by a post-thermal annealing process, as described in the experimental section. To control the pore-to-pore distance or wall thickness, we manipulated the weight ratio (α) of TBT to PS. As shown in Fig. 3(a), the macropores are loosely packed and disordered for α=5. However, for $\alpha \leq 2$, they are closely packed and ordered, as shown in Fig. 3(b)-(d), in which the wall thickness decreases as α decreases (Fig. S2). Because of the high reactivity of TBT, amorphous titania gels are formed around the PS beads during the evaporation process; these gels are solidified in the annealing step. The internal structures of the PS beads in the composite spheres and the macropores

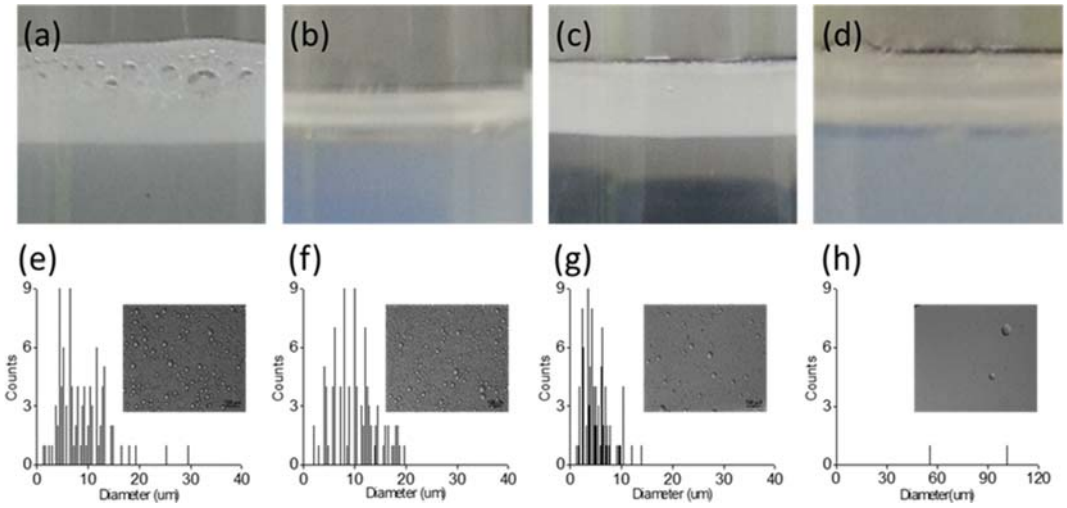

Fig. 2. (a)-(d) Photographs of toluene-in-formamide emulsion stabilized with (a), (b) F108 and (c), (d) P123 surfactants (a), (c) before and (b), (d) after heat treatment. (e)-(h) Size distributions of emulsions with (e), (f) F108 and (g), (h) P123 surfactants (e), (g) before and (f), (h) after heat treatment, as obtained by analyzing optical micrographs (insets).

in the porous spheres are confirmed in TEM imaging (Fig. S2). As shown in the high-magnification TEM images in Fig. S2(a)-(d), as the TBT ratio increases, the pore-to-pore distance in the macroporous TiO_2 spheres is increased; the wall thicknesses are 247, 265, and 280 nm for α=0.5, 1, and 2 (i.e., TBT : PS=1 : 2, 1 : 1, and 2 : 1), respectively. For the precise analysis of the internal structures, we prepared cross-sections of the PS-TiO_2 composite balls using FIB; the sections show hexagonally arranged structures, as shown in Fig. S3.

2. Reflective Colors from Single C-MAC TiO_2 Sphere

Because of Bragg reflections or optical stop bands of the internal ordered structures, our C-MAC TiO_2 spheres show strong light reflections corresponding to their structural periodicity. The wavelength of the reflection peak can be calculated using the modified Bragg Eq. (1) [23,24]:

$$\lambda = \frac{2d_{hkl}}{m}\sqrt{n_{avg}^2 - \sin^2\theta} \quad (1)$$

where λ is the peak of the optical stop band, n_{avg} (=Øn_{sphere}+(1−Ø)$n_{background}$) is the volume fraction-weighted average of the refractive indices of the materials, θ is the angle between the reflected light and the incidence angle, d_{hkl} (=$D\sqrt{2}/\sqrt{h^2+k^2+l^2}$ is the spacing

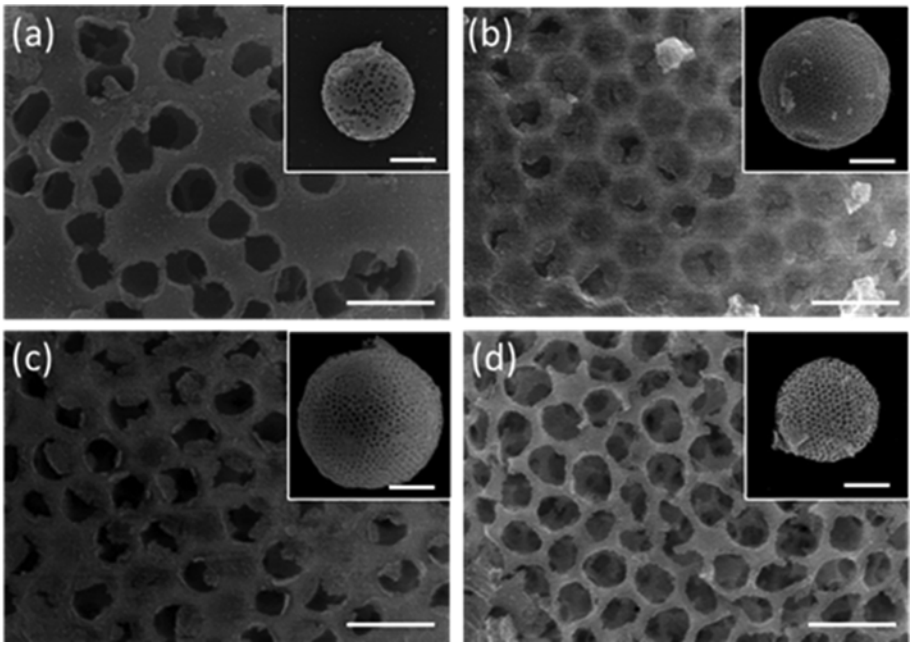

Fig. 3. SEM images of C-MAC TiO_2 spheres from emulsions with different mixing ratios (α) of TBT to 300-nm PS beads (TBT : PS) of (a) 5 : 1, (b) 2 : 1, (c) 1 : 1, and (d) 1 : 2. Scale bars are 500 nm and 2 mm for inset.

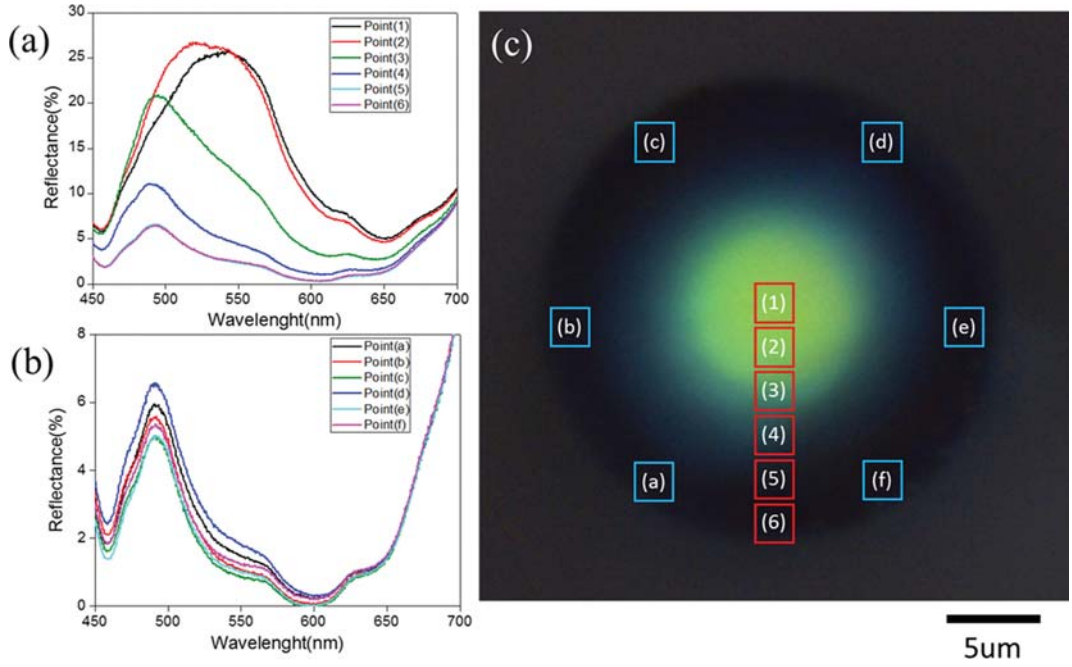

Fig. 4. (a) Reflection spectra of single C-MAC TiO_2 sphere from center to edge of sphere; (b) spectra at five different points near edges in (c) optical micrograph, in which 300-nm TBT and PS beads are mixed with a 2 : 1 mixing ratio and the carbonization temperature of 540 °C.

of the diffraction layers of the fcc lattice structure, h, k, and *l* are the Miller indices of the crystal structure plane, m is the integer representing the order of diffraction considered as first-order, and D is the pore-to-pore distance. Because the densest plane of the fcc lattice is the (111) plane, which is parallel to the surfaces of the C-MAC TiO_2 spheres, their specular surface reflection peak wavelength would be $\lambda = \frac{2D\sqrt{2}}{\sqrt{3}}\sqrt{n_{avg}^2}$.

As shown in Fig. 4, in order to understand how our ordered macroporous spheres reflect light, we measured the reflection spectra from single particles under optical microscopy equipped with spectroscopy at different positions on the C-MAC TiO_2 surface. During the measurement, we fixed the detection area to 15 pixels and measured the reflection spectra of the C-MAC TiO_2 sphere at six different points from the center to the edge. From positions (1), (3), and (6), reflectance peaks are measured at 542 nm, 520 nm, and 480 nm (Fig. 4), matching the predicted peak positions of 555 nm, 532 nm, and 474 nm for the angle values of 0, 29, and 45°, respectively. Here, we assume that the refractive index of the matrix is 2.35, calculated as the average of TiO_2 and carbon depending on the volume ratio of carbon, as confirmed in Fig. S4 [25]. Therefore, the average refractive index of the spheres is calculated as 1.35, including the refractive index of air voids. In Fig. 4, as the detection area moves from (1) to (6), each position shows a different reflection spectrum and intensity because of the angle dependency. However, the reflection spectrum and intensity are unchanged at the same angle. Then, we changed the detection area to investigate the correlation between intensity and angle. As shown in Fig. S5, we measured the ultraviolet-visible (UV/Vis) reflections from different areas of a single sphere. The reflection from inside the square area was approximately 544 nm and 465 nm. When the detection area was enlarged to the red square box, the peak intensity at ~465 nm was increased significantly, while that at 544 nm was increased gradually because of the collection of light back-reflected from a wider range of angles. As the results demonstrate, we can limit the considerable range of angles because the reflection peak is unchanged over 45°, as confirmed by the matching of the measured and calculated peak. The light behavior may be similar to that of a convection mirror. Following these results, the reflection spectrum cannot be perfectly explained by Eq. (2), because the C-MAC TiO_2 sphere has a curved, not flat, surface. For the calculation of the reflection spectrum, we considered the angle dependency.

Because our C-MAC TiO_2 spheres show polydisperse size distributions, the effect of sphere size on the reflection spectrum is investigated, in which the sphere diameter ranges from 16 μm to 20.4 μm (Fig. 5(a)-(d)). The green spot size of the center is increased as the diameter increases and the reflection peaks remain at 540 nm. Even if the diameter is changed, light is reflected at the same wavelength for detection areas with the same position. As the reflection position is moved to the middle and then the central positions, the reflection intensity is decreased. However, the tail of the main peak near 450 nm is increased as the diameter increases, corresponding to the blue zone of back-reflected light from a wider range of angles. For larger particles (Fig. 5(c)-(d)), blue colors are detected at the central position (Fig. 5(g)-(h)). In these results, the C-MAC TiO_2 diameter does not affect the reflection spectrum.

3. Reflective Colors from C-MAC TiO_2 Powder

Previously, we discussed the reflective colors observed from a single sphere at different positions. Here, we confirmed reflective colors from the C-MAC TiO_2 spheres in bulk, which have different

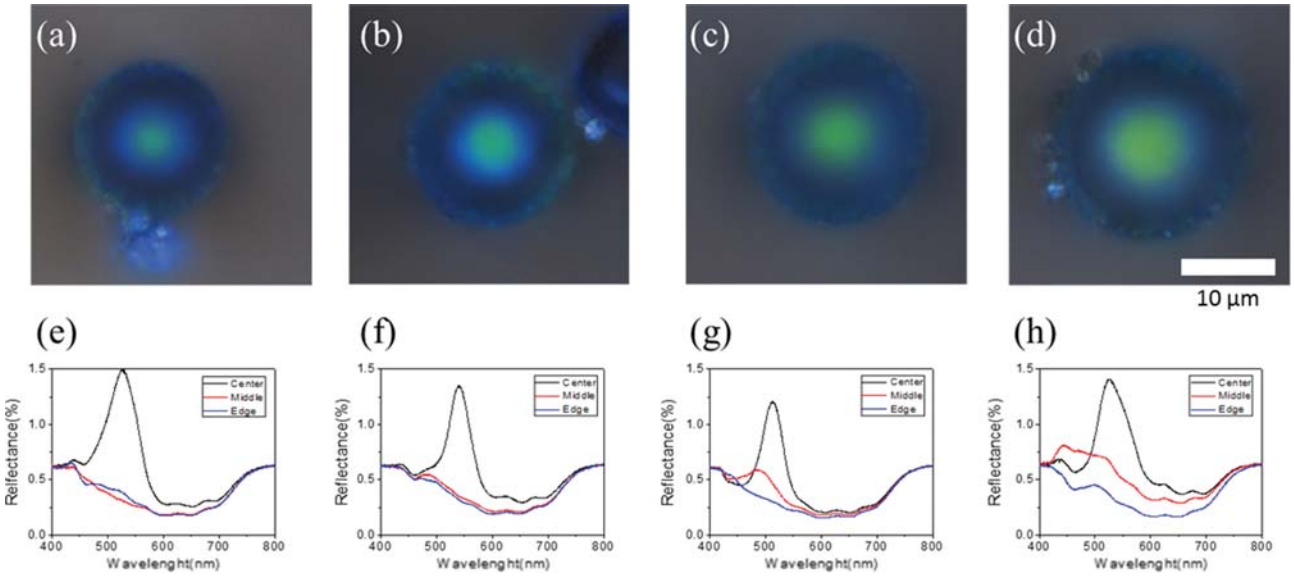

Fig. 5. (a)-(d) Optical micrographs of C-MAC TiO_2 spheres with diameters of (a) 16.5 μm, (b) 18.4 μm, (c) 19.3 μm, and (d) 20.4 μm. (e)-(h) Reflection spectra of three different positions (15 pixel) at center, middle, and edge of four different spheres in (a)-(d), in which TBT and 300-nm PS beads are mixed with 2 : 1 mixing ratio and carbonization temperature is at 540 °C.

periodicities based on the ratio of TBT and PS, calcination temperatures, and PS diameters. First, as the weight ratio of TBT to PS beads increases, thicker TiO_2 walls are formed, increasing the pore-to-pore distance (D) and therefore the periodicity. Thereby, the reflection peak (λ) is shifted to a longer wavelength, as shown in Fig. 6. At the weight ratio of 5 : 1, the macropores are disordered and no Bragg reflection peaks or reflective colors appear in the spectra or photographs, respectively. For the other cases, peaks are measured around 520, 555, and 590 nm for 1 : 2, 1 : 1, and 2 : 1 weight ratios of TBT to PS, respectively, which are slightly shorter than the calculated peak wavelengths of 559, 588, and 623 nm from Eq. (2),

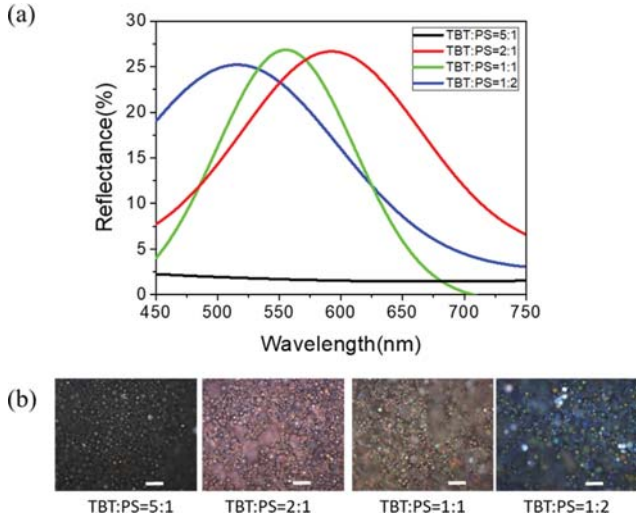

Fig. 6. (a) Reflection spectra and (b) optical micrographs of C-MAC TiO_2 spheres with different mixing ratios of TBT to 300 nm PS beads. Carbonization temperature is 540 °C. Scale bars are 100 μm.

respectively. This discrepancy can be attributed to the angle dependency of reflective color on the curved surfaces of single spheres, as discussed in the previous section.

The pore-to-pore distance and crystalline phase of titania can be controlled by adjusting the thermal annealing temperature. As the annealing temperature is increased, the pore-to-pore distance decreases gradually. When the PS-TiO_2 composite spheres were annealed under nitrogen atmosphere at 540, 700, 800, and 900 °C, the pore-to-pore distances were measured as 292, 286, 286, and 279 nm, respectively. On the other hand, as the annealing temperature was increased, titania was gradually transformed from anatase to rutile, as confirmed in XRD patterns (Fig. S6). Up to 700 °C, both phases of anatase and rutile were detected. However, only the rutile phase was detected at 800 °C and 900 °C. The carbon content in the thermally annealed composite spheres was ~15 wt% and remained unchanged up to 800 °C, but was decreased to 13 wt% at 900 °C, as plotted in Fig. S4.

Because the rutile phase is dense and high in refractive index, the reflection peak from the high-temperature-annealed spheres should be shifted to a longer wavelength. However, the pore-to-pore distance was decreased much more during heat treatment; therefore, the reflection peak was shifted to a slightly shorter wavelength instead. As shown in Fig. 8, the reflection peak wavelengths are decreased from 610 nm to 584 nm as the annealing temperature increases from 540 °C to 900 °C; these values are well matched with those calculated from Eq. (2), assuming that the refractive index is 1.36. Notably, the reflectance peak position was shifted to slightly shorter wavelength and intensity decreased as the annealing temperature increased. We speculate that more rutile-phase titania is grown which and structural disorder is increased slightly at higher annealing temperatures, which may reduce the peak intensity. As shown in the low-magnification optical micrographs in Fig. 8(b)-(e), the color of spheres changed from red-brown for the samples annealed at 540 °C

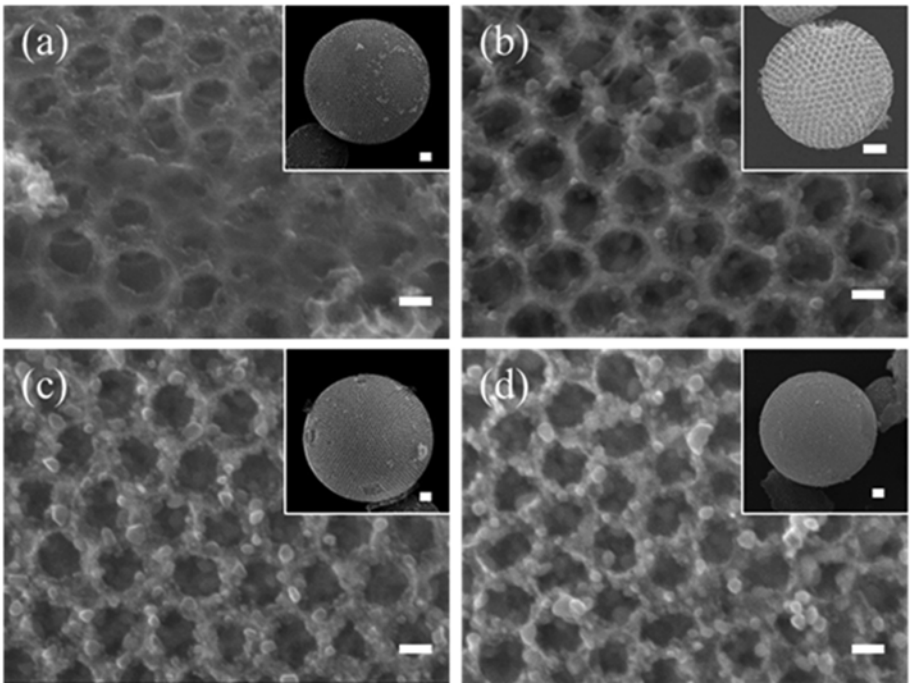

Fig. 7. SEM images of C-MAC TiO_2 spheres depending on carbonization temperatures: (a) 540 °C, (b) 700 °C, (c) 800 °C, (d) 900 °C. Scale bars are 200 nm and 1 μm for insets.

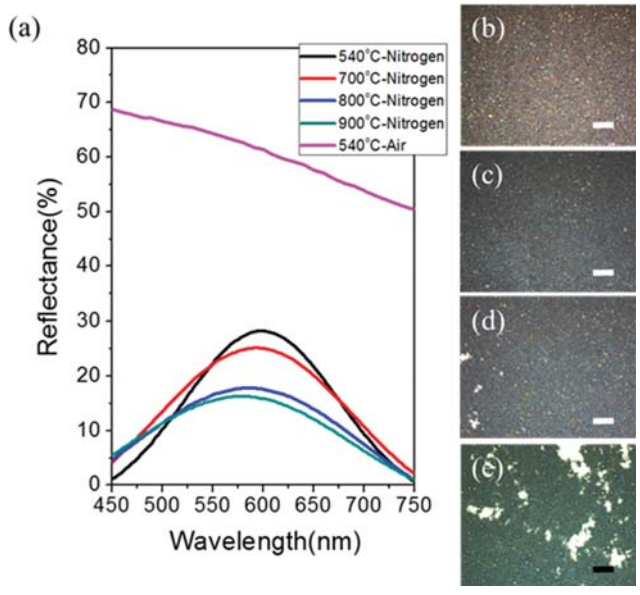

Fig. 8. (a) Reflection spectra of C-MAC TiO_2 spheres annealed at different temperatures under either nitrogen or air atmosphere. (b)-(e) Optical micrographs of C-MAC TiO_2 annealed at (b) 540 °C, (c) 700 °C, (d) 800 °C, and (e) 900 °C under nitrogen atmosphere. Scale bars are 100 μm.

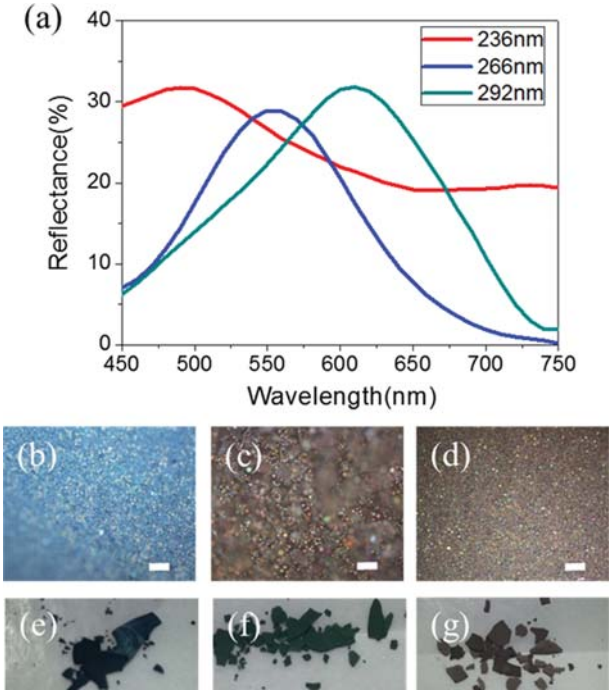

Fig. 9. (a) Normalized reflection spectra of C-MAC TiO_2 spheres which were prepared by co-assembly of TBT and PS in toluene droplets and calcination at 540 °C. (b)-(d) Optical micrographs and (e)-(g) powder images of C-MAC TiO_2 spheres with the pore diameter (d_{pore}) of (b), (e) 236 nm, (c), (f) 266 nm, and (d), (g) 292 nm. Scale bars are 100 μm.

to green for 900 °C, corresponding to the reflection spectra in Fig. 8(a).

Finally, we changed the size of the PS bead as a template to control the pore-to-pore distance (D). As shown in Fig. S7, when PS beads with diameters of 190, 270, 300, and 350 nm were used, the pore-to-pore distances in the C-MAC TiO_2 spheres were measured as 156, 236, 266, and 292 nm, respectively. At the pore-to-pore distance of 156 nm, the color of C-MAC TiO_2 spheres was dark blue,

near the block color, in both optical microscopy and photograph images. The reflective peak was measured as the UV wavelength of 360 nm (Fig. S8). As the pore-to-pore distance was decreased, the reflection of light appeared in the UV range. However, with the pore-to-pore distances of 236, 266, and 292 nm, the optical microscopy images in Fig. 9(b)-(d) and photographs in 9(e)-(g) show the color change of the spheres from blue to red, respectively, which are well matched with the wavelengths of the reflection peaks shown in Fig. 9(a). These results indicate the potential to realize visible- and UV-light reflective materials by controlling the templating material size.

CONCLUSIONS

We prepared thermally stable toluene-in-formamide emulsions stabilized with Pluronic® F108 surfactant (EO_{125}-b-PO_{64}-b-EO_{125}). By encapsulating PS beads within the emulsions, composite spheres were prepared through the slow evaporation of toluene; C-MAC TiO_2 spheres were finally produced by the direct carbonization of PS and organic part of titania precursors. The carbon within the MAC TiO_2 spheres suppressed wavelength-independent multiple scattering. Therefore, Bragg reflection colors in the visible range were observed from powders of the C-MAC TiO_2 spheres; the colors were independent of the rotation angle because of their unique spherical shapes and pore structures. Furthermore, the reflected colors could be controlled by changing the weight ratio of the precursors, the size of polymer beads, and the thermal annealing temperature. Because these materials can be prepared in solution, we believe that they can be further implemented in various applications such as pigments, sensors, dye-sensitized solar cells, catalysts, and others [26-29].

ACKNOWLEDGEMENTS

This work was supported by National Research Foundation of Korea (2014M3A9B8023471, 2017M3A7B8065528, and 2017R1A5A1070259).

SUPPORTING INFORMATION

Additional SEM, TEM images and element analysis, X-Ray diffraction data, UV/Vis reflection spectra, optical micrographs. Additional information as noted in the text. This information is available via the Internet at http://www.springer.com/chemistry/journal/11814.

REFERENCES

1. E. Armstrong and C. O'Dwyer, *J. Mater. Chem., C*, **3**, 6109 (2015).
2. E. R. Dufresne, H. Noh, V. Saranathan, S. G. J. Mochrie, H. Cao and R. O. Prum, *Soft Matter*, **5**, 1792 (2009).
3. M. Xiao, Z. Hu, Z. Wang, Y. Li, A. D. Tormo, N. Le Thomas, B. Wang, N. C. Gianneschi, M. D. Shawkey and A. Dhinojwala, *Sci. Adv.*, **3**, e1701151 (2017).
4. S. F. Leung, Q. Zhang, F. Xiu, D. Yu, J. C. Ho, D. Li and Z. Fan, *J. Phys. Chem. Lett.*, **5**, 1479 (2014).
5. C. Fenzl, T. Hirsch and O. S. Wolfbeis, *Angew. Chem. Int. Ed.*, **53**, 3318 (2014).
6. A. C. Arsenault, D. P. Puzzo, I. Manners and G. A. Ozin, *Nature Photon.*, **1**, 468 (2007).
7. X. Zhang, F. Wang, L. Wang, Y. Lin and J. Zhy, *Dyes Pigm.*, **138**, 182 (2017).
8. T. Chokpanyarat, V. Punsuvon and S. Achiwawanich, *Adv. Mater. Sci. Eng.*, 2018, **1** (2018).
9. F. Liu, B. Shan, S. Zhang and B. Tang, *Langmuir*, **34**, 3918 (2018).
10. M. Zalfani, B. van der Schueren, M. Mahdouani, R. Bourguiga, W.-B. Yu, M. Wu, O. Deparis, Y. Li and B.-L. Su, *Appl. Catal., B*, **199**, 187 (2016).
11. Q. Jiang, L. Wang, C. Yan, Z. Guo and N. Wang, *Eng. Sci.*, **1**, 64 (2018).
12. H. Chen, R. Lou, Y. Chen, L. Chen, J. Lu and Q. Dong, *Drug Deliv*, **24**, 775 (2017).
13. C. Cheng, S. K. Karuturi, L. Liu, J. Liu, H. Li, L. T. Su, A. I. Tok and H. J. Fan, *Small*, **8**, 37 (2012).
14. X. Yan, K. Ye, T. Zhang, C. Xue, D. Zhang, C. Ma, J. Wei and G. Yang, *New J. Chem.*, **41**, 8482 (2017).
15. H. Zhao, W. Deng and Y. Li, *Adv. Com. Hybrid. Mater.*, **1**, 404 (2018).
16. V. N. Manoharan, A. Imhof, J. D. Thorne and D. J. Pine, *Proc. SPIE*, **44**, 3937 (2000).
17. J. P. Schwarz, J. R. Spackman, D. W. Fahey, R. S. Gao, U. Lohmann, P. Stier, L. A. Watts, D. S. Thomson, D. A. Lack, L. Pfister, M. J. Mahoney, D. Baumgardner, J. C. Wilson and J. M. Reeves, *J. Geophy. Res.*, **113**, D03203 (2008).
18. Y. Takeoka, S. Yoshioka, A. Takano, S. Arai, K. Nueangnoraj, H. Nishihara, M. Teshima, Y. Ohtsuka and T. Seki, *Angew. Chem. Int. Ed.*, **52**, 7261 (2013).
19. W. Wang, B. Tang, W. Ma, J. Zhang, B. Ju and S. Zhang, *J. Opt. Soc. Am. A.*, **32**, 1109 (2015).
20. D. P. Josephson, M. Miller and A. Stein, *Z. Anorg. Allg. Chem.*, **640**, 655 (2014).
21. S. M. Klein, V. N. Manoharan, D. J. Pine and F. F. Lange, *Langmuir*, **21**, 6669 (2005).
22. A. Imhof and D. J. Pine, *J. Colloid Interface Sci.*, **192**, 368 (1997).
23. W. H. Bragg and W. L. Bragg, *Proc. Royal Soc., A*, **88**, 428 (1913).
24. C. I. Aguirre, E. Reguera and A. Stein, *Adv. Funct. Mater.*, **20**, 2565 (2010).
25. S.-H. Kim, Y.-S. Cho, S.-J. Jeon, T. H. Eun, G.-R. Yi and S.-M. Yang, *Adv. Mater.*, **20**, 3268 (2008).
26. G. Veerappan, D. W. Jung, J. Kwon, J. M. Choi, N. Heo, G.-R. Yi and J. H. Park, *Langmuir*, **30**, 3010 (2014).
27. Y. B. Kim, T. Tran-Phu, M. Kim, D. W. Jung, G.-R. Yi and J. H. Park, *ACS. Appl. Mater. Interfaces*, **7**, 4511 (2015).
28. H. M. Koo, T. Tran-Phu, G.-R. Yi, C.-H. Shin, C.-H. Chung and J.-W. Bae, *Catal. Sci. Technol.*, **6**, 4221 (2016).
29. X. Yang, C. Liang, T. Ma, Y. Guo, J. Kong, J. Gu, M. Chen and J. Zhu, *Adv. Com. Hybrid. Mater.*, **1**, 207 (2018).

Supporting Information

Scalable synthesis of carbon-embedded ordered macroporous titania spheres with structural colors

Dae-Woong Jung*, Kyung Jin Park, Seungwoo Lee*,**, Jaeyun Kim*, Gaehang Lee***, and Gi-Ra Yi*,†**

*Department of Chemical Engineering, Sungkyunkwan University, Suwon 16419, Korea
**SKKU Advanced Institute of Nanotechnology (SAINT), Sungkyunkwan University, Suwon 16419, Korea
***Korea Basic Science Institute, Daejeon 34133, Korea
(*Received 3 May 2018 • accepted 24 June 2018*)

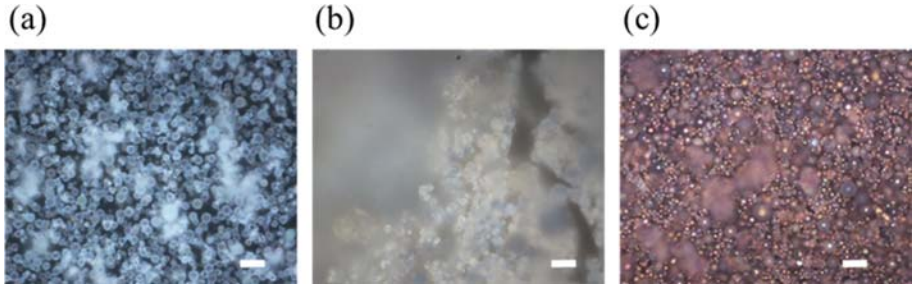

Fig. S1. Optical micrographs of (a) composite balls of PS-TiO_2, (b) MAC TiO_2 spheres and (c) C-MAC TiO_2 Spheres for which 300-nm PS beads and TBT are mixed with 1 : 2 mixing ratio of TBT to PS and carbonization temperature is at 540 °C. Scale bars are 100 μm.

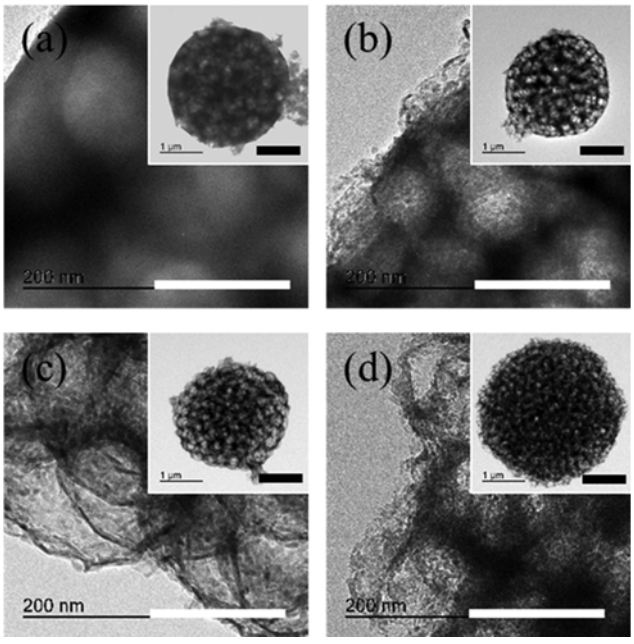

Fig. S2. TEM images of C-MAC TiO_2 spheres obtained from emulsions with different mixing ratios of TBT to 300-nm PS beads (TBT : PS), which are (a) 5 : 1, (b) 2 : 1, (c) 1 : 1, (d) 1 : 2. Scale bars are 200 nm and 1 μm for inset.

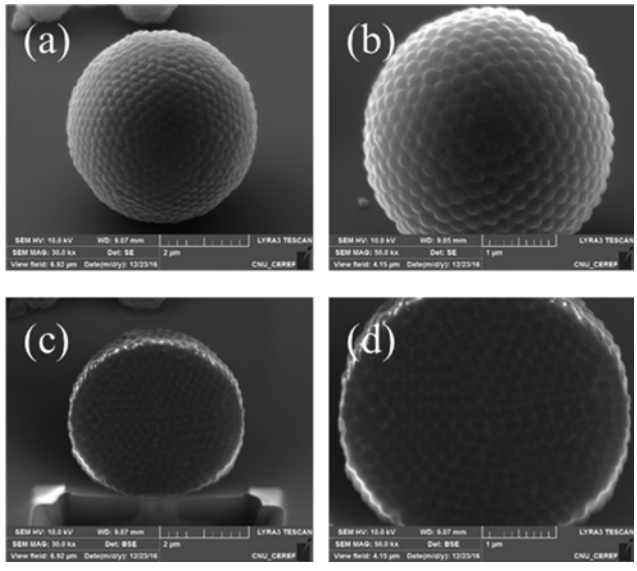

Fig. S3. SEM images of composite ball of PS-TiO_2 with (a), (b) before and (c), (d) after cross-section by FIB and TBT : PS ratio is 1 : 2.

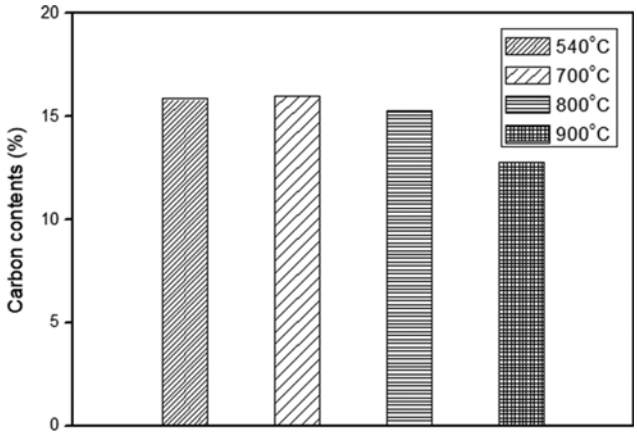

Fig. S4. Element analysis of C-MAC TiO_2 spheres with different carbonization temperatures that are (a) 540 °C, (b) 700 °C, (c) 800 °C, (d) 900 °C.

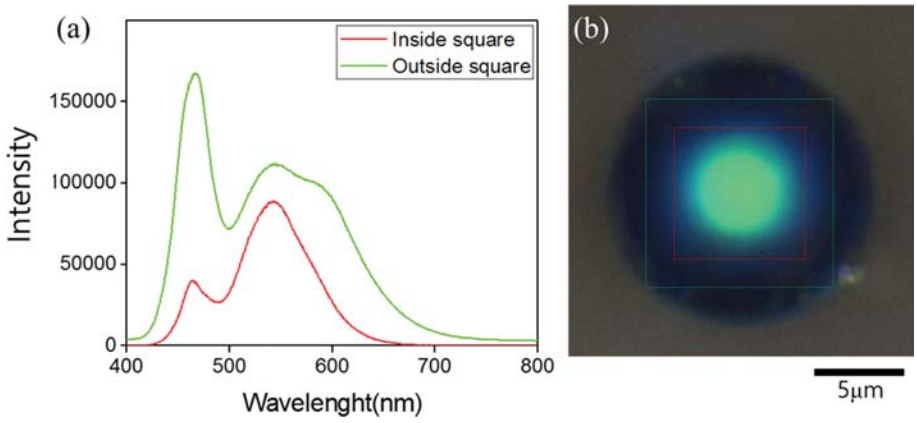

Fig. S5. (a) Reflection spectra of single C-MAC TiO_2 sphere from red and green squares near center of spheres in (b) optical micrograph, for which 300-nm PS beads and TBT are mixed with 1 : 2 mixing ratio of TBT to PS and carbonization temperature is 540 °C.

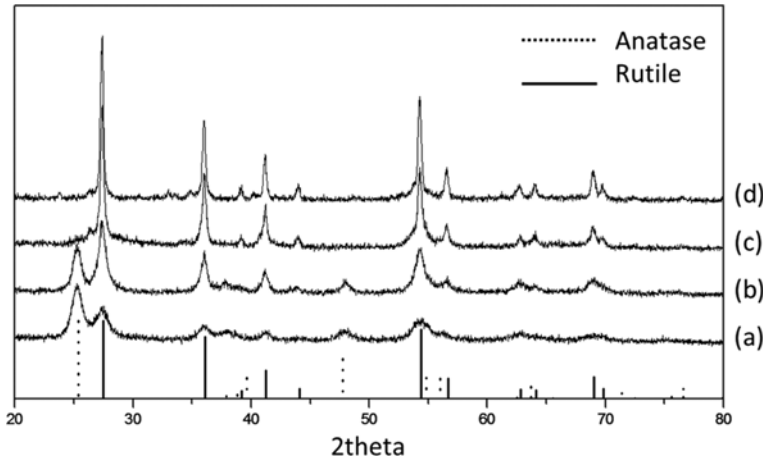

Fig. S6. Change of X-ray diffraction patterns of C-MAC TiO_2 spheres with different carbonization temperatures which are (a) 540 °C, (b) 700 °C, (c) 800 °C, (d) 900 °C.

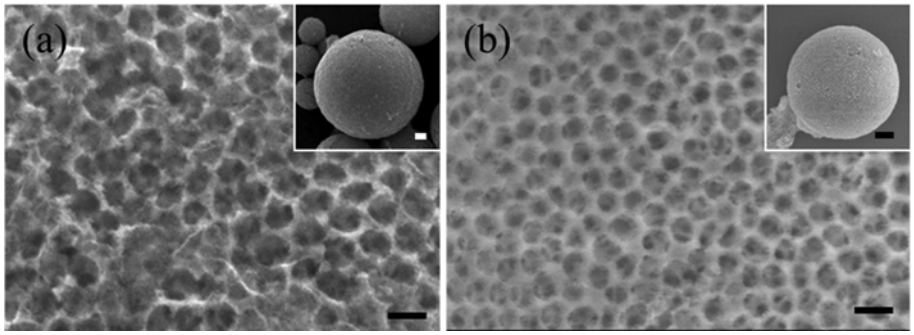

Fig. S7. SEM images of C-MAC TiO_2 spheres from emulsions with different pore diameters which are (a) 236 nm and (b) 157 nm. Mixing ratio of TBT to PS beads is 1 : 2 and calcination at 540 °C. Scale bars are 200 nm and 1mm for insets.

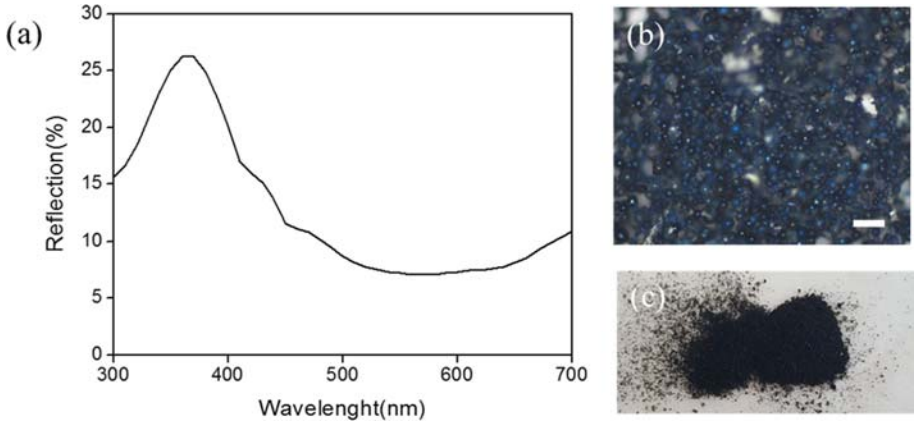

Fig. S8. (a) Normalized reflection spectra of C-MAC TiO_2 spheres which were prepared by co-assembly of TBT and PS (1 : 2 ratio) in the toluene droplets and calcination at 540 °C. (b) Optical micrographs and (c) powder images of C-MAC TiO_2 spheres with the pore diameter (d_{pore}) of 156 nm. Scale bar is 100 μm.